

## GENERATION METHOD OF BROADBAND STATISTICAL GREEN'S FUNCTIONS FOR BOTH HORIZONTAL AND VERTICAL GROUND MOTIONS

T. Satoh<sup>1</sup>

<sup>1</sup> Senior Researcher, Institute of Technology, Shimizu Corporation, Tokyo, Japan  
Email: toshimi.satoh@shimz.co.jp

### ABSTRACT :

In the statistical (stochastic) Green's function method for P-wave have in the near source region not been studied very much. In addition, statistical Green's functions of vertical ground motions have not been verified by strong motion records. In this study generation method of broadband statistical Green's functions of horizontal and vertical ground motions for both P and S-waves is proposed. The method is verified by comparing the generated statistical Green's functions with strong motion records of a crustal earthquake ( $M_w=4.9$ ) observed at 13 stations in Japan. The proposed method reproduced the observed records in general.

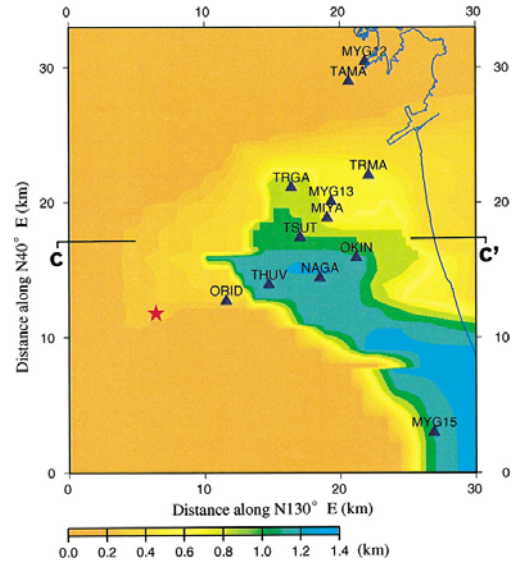
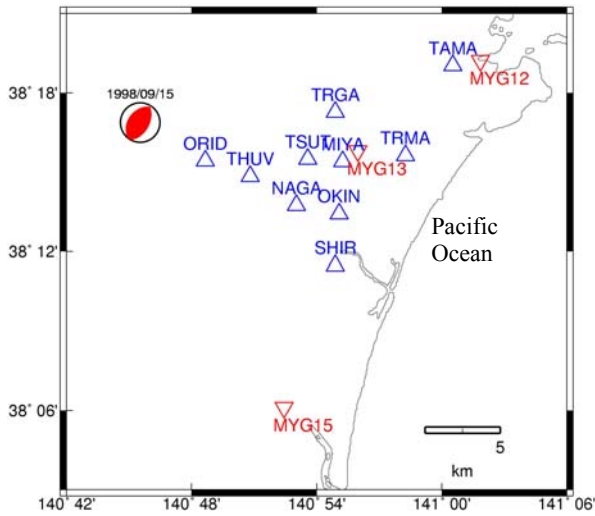
**KEYWORDS:** Strong motion prediction, Green's function, vertical motions, near-field, scattering

### 1. INTRODUCTION

The statistical (stochastic) Green's function method (Kamae et al., 1991; Satoh et al., 1994) has been widely used for strong motion prediction by many organizations, such as government and local self-governing body in Japan. However, only S-waves have been predicted and P-waves in the near source region have not been studied very much in the statistical Green's function method. In addition, statistical Green's functions of vertical ground motions have not been verified by strong motion records of middle-sized earthquakes. In "Regulatory Guide for Reviewing Seismic Design of Nuclear Power Reactor Facilities" revised in 2006, the necessity of the prediction of vertical ground motions by using fault models was newly included. Therefore generation method of broadband statistical Green's functions of horizontal and vertical ground motions for both P and S-waves in the near source region is proposed in this study. Then the method is verified by comparing the generated statistical Green's functions with strong motion records of a crustal earthquake ( $M_w=4.9$ ) observed at 13 stations in the hypocentral distance range from 13.5 to 27.1 km.

### 2. DATA

In Figure 1 (a) the epicenter (Tohoku University, 1999) and the mechanism (F-net) of the 1998 Miyagiken-Nambu earthquake are shown together with 13 strong motion stations in and around the Sendai basin, Japan. The seismic moment estimated by F-net is  $3.19 \times 10^{23}$  dyne-cm ( $M_w=4.9$ ) and the focal depth is 12.4 km (Tohoku University, 1999). Stations MIYA, TAMA, ORID, TSUT, OKIN, TRMA, TRGA, NAGA, and SHIR have been deployed as a cooperative research between the Building Research Institute and the Association for Promoting of Building Research. Station THUV has been deployed jointly by Shimizu Corporation and Tohoku University. Stations MYG12, MYG13, and MYG15 have been deployed by the National Research Institute for Earth Science and Disaster Prevention (NIED) as a part of K-NET Three dimensional basin structure up to the engineering bedrock with the S-wave velocity of 500 m/s has been constructed through three dimensional finite-difference waveform modeling of the same strong motion records of this earthquake from the initial model estimated using array and single station microtremor records (Satoh et al., 2001a, 2001b). The depth contour of the seismic bedrock with S-wave velocity of 3,000 m/s is shown in Figure 1 (b). The S-wave velocity structure and the damping factor above the engineering bedrock have been estimated by an inversion method using surface and borehole records (Satoh et al., 1995) except for MYG12, MYG13, and MYG15. The subsurface structure at MIYA is shown in Table 2.1 as an example. The seismic bedrock depth at MIYA is 650 m (Satoh et al., 2001b).



(a) Epicenter and stations used in this study

(b) Bedrock depth estimated by Satoh et al. (2001b)

Figure 1 Location of the epicenter (Tohoku University, 1999) and mechanism (F-net by NIED) of the 1998 Miyagiken-Nambu earthquake, Japan together with strong motion stations.

Table 2.1 Subsurface structure at MIYA

No.	Thicknes (m)	$V_p$ (m/s)	$V_s$ (m/s)	Daming factor ( $h = h_0 f^{-\alpha}$ )		Density (g/cm <sup>3</sup> )
				$h_0$	$\alpha$	
1	1.5	380.0	203.3	0.5600	0.84	1.6
2	1.5	580.0	343.1	0.5600	0.84	1.9
3	4.0	1000.0	419.5	0.5600	0.84	1.9
4	4.0	1200.0	419.5	0.5600	0.84	1.9
5	50.0	1800.0	500.0	0.0071	1.00	2.0
6	200.0	2000.0	850.0	0.0050	1.00	2.1
7	400.0	3300.0	1700.0	0.0033	1.00	2.3
8	6650.0	5500.0	3000.0	0.0025	1.00	2.5
9	9600.0	6000.0	3550.0	0.0025	1.00	2.6
10	2100.0	6600.0	3700.0	0.0010	1.00	2.9

### 3. GENERATION METHOD OF THREE-COMPONENT STATISTICAL GREEN'S FUNCTION

#### 3.1. Spectrum on the seismic bedrock

Complex acceleration Fourier spectrum of a statistical Green's function  $A_{\theta\phi}(f)$  for longitude and latitude directions and  $A_r(f)$  for radial direction on the seismic bedrock can be represented by the equations (3.1) and (3.2), respectively.

$$A_{\theta\phi}(f) = F_s S_s(f) N_{\theta\phi}(f) P_s(f) \quad (3.1)$$

$$A_r(f) = F_p S_p(f) N_r(f) P_p(f) \quad (3.2)$$

Here  $f$  is the frequency (Hz). Subscript  $\theta\phi$  denotes the longitude and latitude direction. Subscript  $r$  denotes the radial direction. Subscript  $S$  and  $P$  denote S-wave and P-wave, respectively.  $F$  is the free surface effects.  $S(f)$  is the acceleration source spectrum for far-field term. The  $N(f)$  is the ratio of near-field and intermediate-field, and far-field terms with respect to the far-field term.  $P(f)$  is the path spectrum. More detail explanations are shown in the sections from 3.2 to 3.4.

#### 3.2. Source spectrum

The Fourier amplitude spectrum of  $S_s(f)$  is given by the relation,

$$|S_s(f)| = C \frac{(2\pi f)^2 M_0}{1 + \left(\frac{f}{f_0}\right)} \left[ 1 + \left(\frac{f}{f_{max}}\right)^m \right]^{-1/2}, \quad (3.3)$$

where  $C$  is given by the following equation:

$$C = \frac{R_{\theta\phi}(f)}{4\pi\rho\beta^3} \sqrt{\frac{\rho\beta}{\rho_z\beta_z}}. \quad (3.4)$$

Here  $M_0$  is the seismic moment,  $f_0$  is the corner frequency, and  $f_{max}$  is the cutoff frequency. The  $f_0$  and  $f_{max}$  are estimated to be 1.29 Hz and 7.9 Hz using transverse components with S-wave observed at 13 stations. In this estimation the amplification factors from the seismic bedrock to the surface are calculated based on one-dimensional wave propagation theory using obliquely incident SH wave with incidence angles estimated by the ray theory. The resultant Brune's (1970) stress drop  $\Delta\sigma$  is 122 bar. The  $m$  is assumed to be 4.2 (Sato et al., 1997). In the equation (3.4),  $\rho$  and  $\beta$  is the density and S-wave velocity at the source ( $\rho=2.6$  g/cm<sup>3</sup>,  $\beta=3.55$  km/s).  $\rho_z$  and  $\beta_z$  is the density and S-wave velocity at the bedrock ( $\rho=2.5$  g/cm<sup>3</sup>,  $\beta=3.0$  km/s).  $R_{\theta\phi}(f)$  is the frequency dependent radiation pattern for S-wave, which was proposed by Sato (2002) analyzing the same records used in this study. The radiation patterns at frequencies lower than 3 Hz are theoretical values and those at frequencies higher than 6 Hz are the same values for three components as the average radiation patterns. The average radiation patterns are calculated by the method by Boore and Boatwright (1984). The resultant average radiation patterns for P wave and S wave are 0.266 and 0.695, respectively. Here the take off angle range is assumed to be from 110 to 150 degrees which correspond to the range at 13 stations. For P-wave,  $|S_p(f)|$  is represented by replacing  $f_0$  to  $\alpha/\beta f_0$  in the equation (3.3) based on Hanks and Wyss (1972) in the same way to Dan et al.(1990). The frequency dependent radiation pattern for P-wave  $R_r(f)$  is assumed in the similar manner to  $R_{\theta\phi}(f)$  except for that the average radiation patterns for horizontal components are assumed to be 2<sup>0.5</sup> times of vertical components. The Fourier phase for the source spectrum is generated using Boore's envelope model (1983). We use the Kagawa's method (2004) in order to generate bell-shape displacement waveform.

The  $N_{\theta\phi}(f)$  in the equation (3.5) is the ratio of near-field and intermediate-field, and far-field terms with respect to the far-field term for longitude and latitude directions derived by Nozu (2006). By the same idea  $N_r(f)$  in the equation (3.6) for the radial direction is derived in this study.

$$N_{\theta\phi}(\omega) = 6iR_\beta^3(1 - e^{-i\omega X(1/\alpha - 1/\beta)}) + 6R_\beta^2(1 - R_0 e^{-i\omega X(1/\alpha - 1/\beta)}) - 3iR + 2iR_\beta R_0^2 e^{-i\omega X(1/\alpha - 1/\beta)} + 1 \quad (3.5)$$

$$N_r(\omega) = -9iR_\alpha^3(e^{-i\omega X(1/\beta - 1/\alpha)} - 1) + 9R_\alpha^2(1/R_0 e^{-i\omega X(1/\beta - 1/\alpha)} - 1) - 4iR_\alpha + 3iR_\alpha / R_0^2 e^{-i\omega X(1/\beta - 1/\alpha)} + 1 \quad (3.6)$$

Here  $\omega=2\pi f$ ,  $R_\beta=\beta/(X\omega)$ ,  $R_\alpha=\alpha/(X\omega)$ , and  $R_0=\beta/\alpha$ . The S-wave velocity  $\beta$  is 3.55 km/s and the P-wave velocity  $\alpha$  is 6 km/s.  $X$  is the hypocentral distance.

### 3.4. Path spectrum

The Fourier amplitude spectrum of  $P_s(f)$  is given by the relation,

$$|P_s(f)| = \frac{1}{X} \exp\left(\frac{-\pi f X}{Q_s V_s}\right) \quad (3.7)$$

Here  $Q_s$  is the quality factor for S-wave and  $V_s$  is the S-wave velocity for the path. For P-wave,  $|P_p(f)|$  is

represented by replacing the subscript  $s$  to  $p$  in the equation (3.7).  $V_s$  and  $V_p$  are 3.55 km/s and 6 km/s, respectively.  $Q_s=50f$  and  $Q_p=100f$  are assumed. Fourier phase spectrum at frequencies higher than 3 Hz is generated using the envelope model based on the scattering theory (Saito et al, 2002; Satoh, 2004) for both P and S-waves. The parameter  $\varepsilon^2/a$  which is the key parameter for this envelope model is assumed to be  $10^{-2} \text{ km}^{-1}$  referring to Yoshimoto et al. (1994). Here  $\varepsilon$  is the root-mean-square value of the fractional velocity fluctuation and  $a$  is the correlation distance. Fourier phase spectrum at frequencies lower than 3 Hz is set to be zero.

### 3.5. Site-specific amplification spectrum

$A_{\theta\phi}(f)$  is distributed into radial, transverse, and vertical components at the upper boundary of the seismic bedrock using the incidence angle computed based on the ray theory. Then the statistical Green's functions for far-field S-wave on the sediments are generated by convolving amplification factors from the seismic bedrock to surface to the far-field term of  $A_{\theta\phi}(f)$ . The final statistical Green's function for S-wave on the sediments are given by adding the far-field S-wave on the sediments and the near-field and intermediate -field S-wave on the bedrock. The statistical Green's functions for P-wave at the surface are generated in the same way. Finally the generated Green's functions for P-wave and S-wave are summed up in the time domain.

As the amplification factors, the following four cases are assumed.

- ① One-dimensional amplification factors with oblique incidence angle calculated based on the ray theory.
- ② One-dimensional amplification factors with vertically incident S-wave for radial and transverse components. One-dimensional amplification factor with vertically incident P-wave for vertical component.
- ③ One-dimensional amplification factors with oblique incidence angle with 30 degree.
- ④ ① at frequencies lower than 3 Hz. ③ at frequencies higher than 6 Hz. Hybrid of Green's functions generated using ① and ② at the frequency range from 3 to 6 Hz.

## 4. VERIFICATION OF THE METHOD USING OBSERVED RECORDS

### 4.1. Statistical Green's function on the seismic bedrock

Figure 2 compares displacements computed by frequency-wave number code (Saikia, 1994) with those statistical Green's functions on the seismic bedrock at MIYA and ORID. All the displacements have been

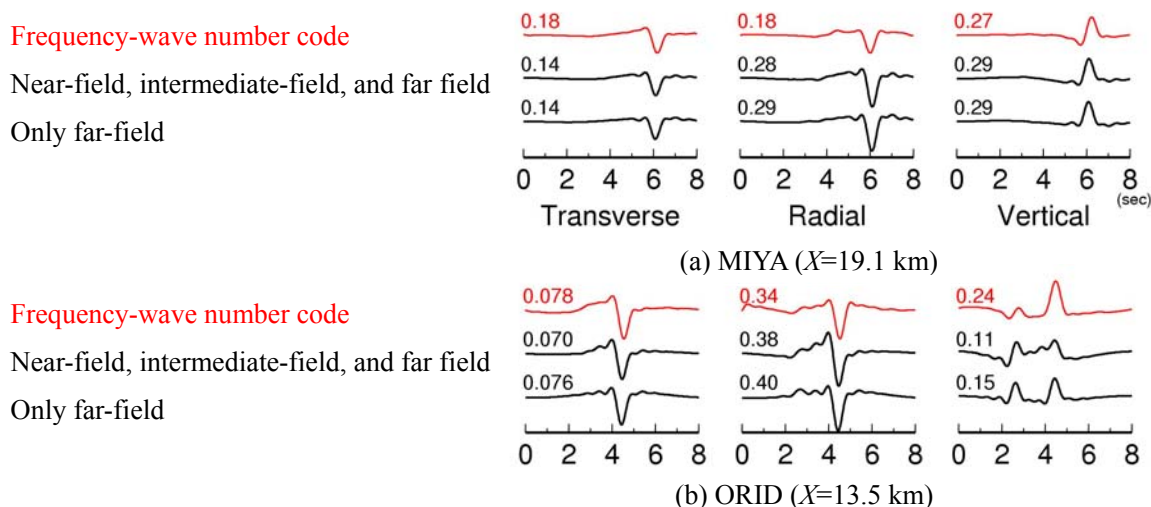


Figure 2 Comparison of displacements computed by frequency-wave number code by Saikia (1994) (top traces) with those of the statistical Green's functions (middle and bottom traces) on the bedrock. The peak amplitude is indicated above each trace.

band-pass filtered from 0.2 to 1.5 Hz. The source duration  $\tau=0.79$  sec used in the frequency-wave number code is given by the relation of  $\tau=2.69\lambda/\beta$ . Here the source radius  $\lambda$  is given by the relation of  $\Delta\sigma=7M_0/(16\lambda^3)$ . The generated Green's functions reasonably agree with the computed ones. The difference between the Green's functions generated considering and not considering near-field and intermediate-field terms is small, because the hypocentral distances of 19.1 km at MIYA and 13.5 km at ORID are not so small. In Figure 3  $N_{\theta\phi}(f)$  and  $N_r(f)$  with  $X=15$  km are shown together with  $N_{\theta\phi}(X\omega/\beta)$  and  $N_r(X\omega/\alpha)$  computed from the equations (3.5) and (3.6). The effects of near-field and intermediate-field terms are not negligible at frequencies lower than about 0.2 Hz for  $N_{\theta\phi}(f)$  and 0.4 Hz for  $N_r(f)$ .

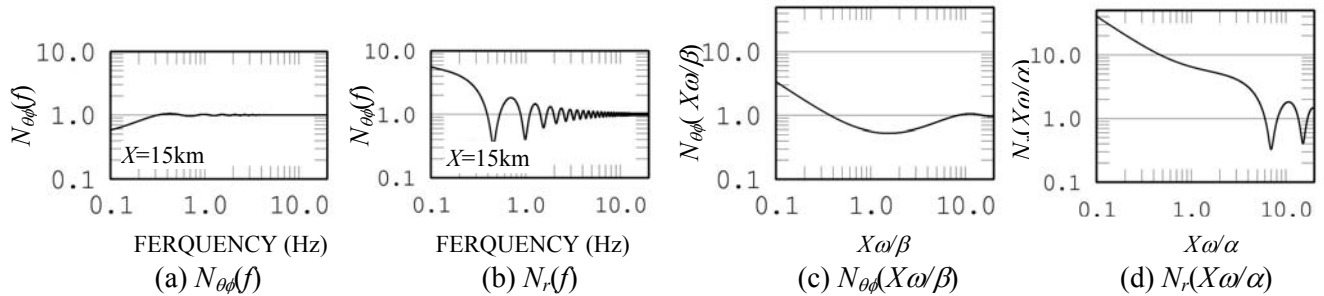


Figure 3  $N_{\theta\phi}(f)$ ,  $N_r(f)$ ,  $N_{\theta\phi}(X\omega/\beta)$  and  $N_r(X\omega/\alpha)$

#### 4.2. Statistical Green's function on the sediments

Figure 4 shows three types of amplification factors of ①, ②, and ③ at MIYA defined in the section 3.5. The incidence angle at the bedrock calculated based on the ray theory is 45 degree for S-wave and 48 degree for P-wave. The difference of three amplification factors for transverse component is smallest among radial, transverse, and vertical components for S-wave. The difference of three amplification factors for vertical component is largest among three components for S-wave. For P-wave the amplification factors in the case of ① have a large peak at the low frequency range, which corresponds to the predominant frequency of S-wave converted from the P-wave.

Figure 5 compares the peak ground accelerations (PGAs) and peak ground velocities (PGVs) of observed records and those of the statistical Green's functions on the sediments generated using four types of amplification factors of ①, ②, ③, and ④ at 13 stations. All of the PGAs and PGVs are for S-waves band-pass filtered from 0.2 to 10 Hz. The vertical bars indicate the range between the average + standard deviation and the average - standard deviation of statistical Green's functions generated using eleven random numbers. The difference of the PGAs and PGVs for the statistical Green's functions using four types of amplification factors is small for transverse and radial components. The PGAs and PGVs for the statistical Green's functions reasonably agree with observed ones for transverse components. The features of observed records that the PGAs and PGVs of radial components are larger than those for transverse components at many stations are reproduced well by the statistical Green's functions with frequency-dependent radiation patterns.

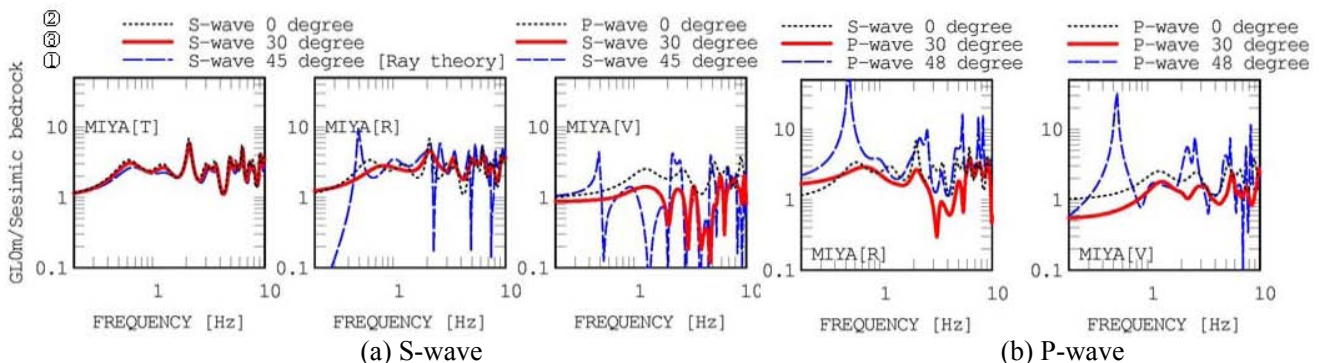


Figure 4 Computed amplification factors from the seismic bedrock to surface on the sediments at MIYA. T, R, V denote transverse, radial, and vertical components. See text in section 3.5 in terms of ①, ②, ③.

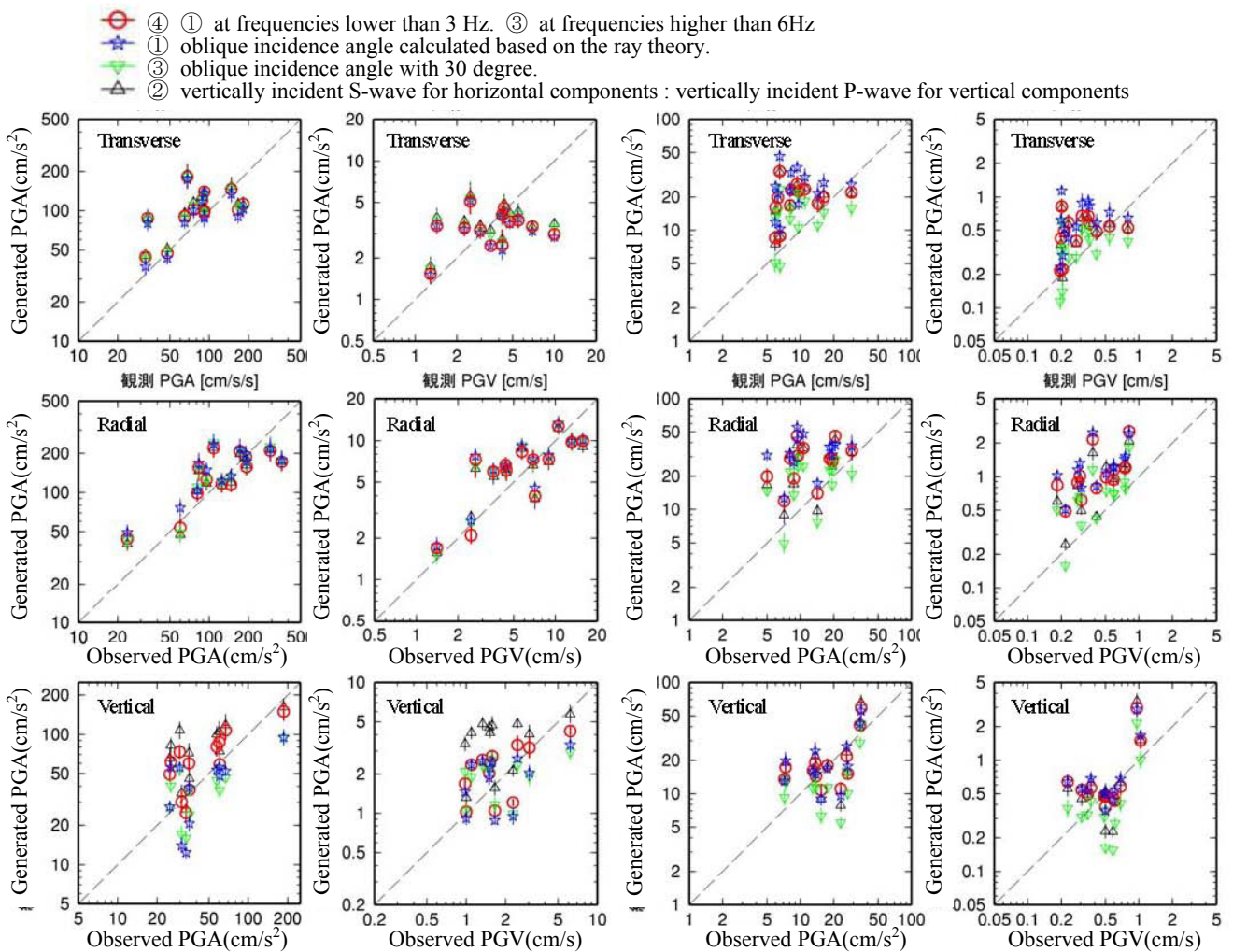


Figure 5 Comparison of PGAs and PGVs of observed records with those of the statistical Green's functions for S-wave.

Figure 6 Comparison of PGAs and PGVs of observed records with those of the statistical Green's functions for P-wave.

For vertical components the PGAs and PGVs for the statistical Green's functions using the amplification factors ① with oblique incidence angle calculated based on the ray theory tend to smaller than observed ones. The PGAs and PGVs for the statistical Green's functions using the amplification factors ③ with oblique incidence angle of 30 degree also tend to smaller than observed ones. On the other hand the PGAs and PGVs for the statistical Green's functions using the amplification factors ④ agree with the observed ones on the average. This result can be interpreted that the effects of incoherent waves such as scattering waves are large at the high frequency range and so the theoretical amplification factors assuming homogeneous media cannot reproduce observed amplification factors at the high frequency range.

Figure 6 is the same as Figure 5 except for P-wave. For transverse and radial components the PGAs and PGVs for the statistical Green's functions using any amplification factors overpredict the observed ones. For vertical components the PGAs and PGVs for the statistical Green's functions using any amplification factors agree with observed ones.

Figure 7 compares observed records with the statistical Green's functions generated using amplification factors (4) at MIYA. All of the velocity waves are band-pass filtered from 0.2 top 10 Hz. The statistical Green's functions reproduce the observed waves in general. However, the statistical Green's functions which consider only body waves could not reproduce later phases at stations such as NAGA and THUV on deep sediments.

The statistical Green's functions shown in Figures 5 to 7 are generated using the envelope model based on the

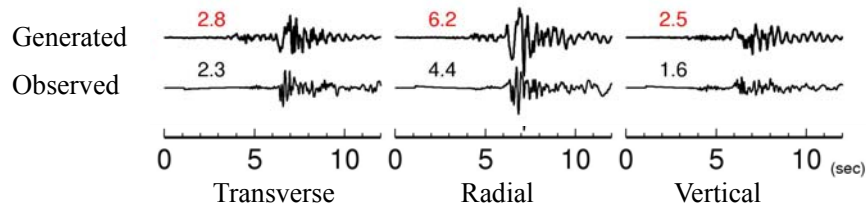


Figure 7 Comparison of observed velocity records (bottom traces) with those of the statistical Green's functions (top traces) at MIYA. The amplification factor ④ is used for the generation of the statistical Green's functions. The peak amplitude is indicated above each trace.

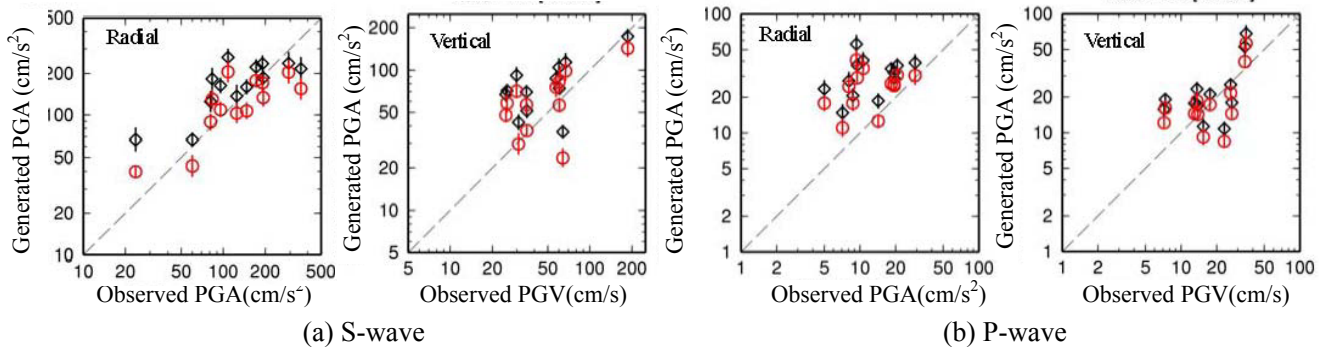


Figure 8 Comparison of PGAs of observed velocity records with those of the statistical Green's functions at MIYA, which are generated considering (○) and not considering (◇) the envelope model based on the scattering theory.

scattering theory at frequencies higher than 3 Hz. In order to examine the validity of this envelope model, we compare the statistical Green's functions generated considering and not considering the envelope model based on the scattering theory. The PGAs of the statistical Green's functions generated not considering the envelope model overpredict the observed ones. On the other hand, the PGAs of the statistical Green's functions considering the envelope model reproduce the observed ones except for radial components for P-wave. This result suggests that the  $\varepsilon^2/a=10^{-2}$  referring to Yoshimoto et al. (1997) is appropriate value. Thus the envelope model based on the scattering theory is useful to generate statistical Green's functions for S-wave and vertical components of P-wave. Frequency-dependent of radiation patterns, envelope as well as amplification factors for P-wave have not been studied very much, so we need to study farther to generate the reasonable statistical Green's functions for horizontal components of P-wave.

## 5. CONCLUSIONS

Generation method of broadband statistical Green's functions of horizontal and vertical ground motions for both P and S-waves in the near source region is proposed in this study. The method is verified by comparing the generated statistical Green's functions with strong motion records of an crustal earthquake with  $M_w=4.9$  in Japan observed at 13 stations in the hypocentral distance range from 13.5 to 27.1 km in Japan. The proposed method reproduces the observed records in general, though the generated Green's functions of horizontal components for P-wave overpredict the observed records. We need to study farther to generate the reasonable statistical Green's functions of horizontal components for P-wave.

## ACKNOWLEDGEMENTS

This research was supported by the Ministry of Education, Science, Sports and Culture, Grant-in-Aid for Scientific Research (C), 20560544 in 2008. We used strong-motion records and P-S-logging results obtained by an array observation project, which was deployed as a cooperative research between the Building Research

Institute and the Association for Promoting of Building Research. We used K-Net strong-motion records and P-S-logging results from NIED. We also used source parameters of F-net by NIED. Several figures were plotted with Generic Mapping Tools (GMT) by Wessel and Smith (1998).

## REFERENCES

- Dan, K., T. Watanabe, T. Tanaka, and R. Sato (1990). Stability of earthquake ground motion synthesized by using different small-event records as empirical Green's functions, *Bull. Seism. Soc. Am.*, **80**, 1433-1455.
- Boore, D. M. (1983). Stochastic simulation of high-frequency ground motions based on seismological models of the radiated spectra, *Bull. Seism. Soc. Am.*, **73**, 1865-1894.
- Boore, D. M. and J. Boatwright (1984). Average body-wave radiation coefficient, *Bull. Seism. Soc. Am.*, **74**, 1615-1621.
- Brune, J. N. (1970). Tectonic stress and the spectra of seismic shear waves from earthquakes, *J. Geophys. Res.*, **75**, 4997-5009.
- Hanks, T. C. and M. Wyss (1972). The use of body-wave spectra in the determination of seismic-source parameters, *Bull. Seism. Soc. Am.*, **62**, 561-589.
- Kamae, K., K. Irikura, and Y. Fukuchi (1991). Prediction of strong ground motion based on scaling law of earthquake, By stochastic synthesis method, *Journal of Struct. Constr. Engng.*, AIJ, **430**, 1-9(in Japanese with English abstract).
- Kagawa, T. (2004). Developing a stochastic Green's function method having more accuracy in long period range to be used in the hybrid method, *Journal of Japan Association for Earthquake Engineering*, **4:2**, 21-32(in Japanese with English abstract).
- Nozu, A. (2006). A simple scheme to introduce near-field and intermediate-field terms in stochastic Green's functions, *Proc. of 12th Japan Earthquake Engineering Symp.*, 190-194 (in Japanese with English abstract).
- Saikia, K. (1994). Modified frequency-wavenumber algorithm for regional seismograms using Filon's quadrature: modeling of Lg waves in eastern North America, *Geophysical Journal International*, **118**, 142-158.
- Saito, T., H. Sato, and M. Ohtake (2002). Envelope broadening of spherically outgoing waves in three-dimensional random media having power law spectra, *J. Geophys. Res.*, **107**, 101029/ 2001JB000264, 3-1-3-16.
- Satoh, T., H. Kawase, and T. Sato (1994). Strong motion prediction considering both non-linear behavior of soil and the statistical characteristics of ground motions extracted from observed data, *Journal of Struct. Constr. Engng.*, AIJ, **463**, 27-37 (in Japanese with English abstract).
- Satoh, T., H. Kawase, and T. Sato (1995). Evaluation of local site effects and their removal from borehole records observed in the Sendai region, Japan, *Bull. Seism. Soc. Am.*, **85**, 1770-1789.
- Satoh, T., H. Kawase, and T. Sato (1997). Statistical spectral model of earthquakes in the eastern Tohoku district, Japan based on the surface and borehole records observed in Sendai, *Bull. Seism. Soc. Am.*, **87**, 446-462
- Satoh, T., H. Kawase, and S. Matsushima (2001a). Estimation of S-wave velocity structures in and around the Sendai basin, Japan using array records of microtremors, *Bull. Seism. Soc. Am.*, **91**, 206-218.
- Satoh, T., H. Kawase, T. Sato, and A. Pitarka (2001b). Three-dimensional finite-difference waveform modeling of strong motions observed in the Sendai basin, Japan, *Bull. Seism. Soc. Am.*, **91**, 812-825.
- Satoh, T. (2002). Empirical frequency-dependent radiation pattern of the 1998 Miyagiken-Nanbu earthquake in Japan, *Bull. Seism. Soc. Am.*, **92**, 1032-1039.
- Satoh, T. (2004). Study on envelope model of ground motions based on inversion of group delay time and scattering theory, *Journal of Struct. Constr. Engng.*, AIJ, **586**, 71-78 (in Japanese with English abstract).
- Tohoku University (1999). Microearthquake activity in and around the Tohoku District (May–October, 1998), *Report of the Coordinating Committee for Earthquake Prediction*, Geophysical Survey Institute, Ministry of Construction, Japan., **61**, 24-43 (in Japanese).
- Wessel, P. and W. H. F. Smith (1998). New, improved version of Generic Mapping Tools released, EOS, AGU
- Yoshimoto, K., H. Sato, and M. Ohtake (1997). Short-wavelength crustal heterogeneities in the Nikko area, Central Japan, revealed from the three-component seismogram envelope analysis, *Physics of the Earth and Planetary Interiors*, **104**, 63-73.